Open access • Posted Content • DOI:10.1101/2020.03.16.994541

Cerebellar modulation of gamma coherence between prefrontal cortex and hippocampus during spatial working memory decision making — Source link

Yu Liu, Samuel S. McAfee, Roy V. Sillitoe, Detlef H. Heck

Institutions: University of Tennessee, St. Jude Children's Research Hospital

Published on: 18 Mar 2020 - bioRxiv (Cold Spring Harbor Laboratory)

Topics: Prefrontal cortex, Spatial memory, Coherence (statistics) and Hippocampus

Cerebellar modulation of prefrontal-hippocampal gamma coherence during spatial working memory decisions

Liu Y[1], McAfee SS[2], Sillitoe RV[3,4,5,6], Heck DH[1]

[1]Department of Anatomy and Neurobiology, University of Tennessee HSC, Memphis, TN 38163, USA

[2]Department of Diagnostic Imaging, St Jude Children's Research Hospital, Memphis, TN, 38112, USA

[3]Department of Pathology and Immunology, Baylor College of Medicine

[4]Department of Neuroscience, Baylor College of Medicine

[5]Development, Disease Models & Therapeutics Graduate Program, Baylor College of Medicine

[6]Jan and Dan Duncan Neurological Research Institute of Texas Children's Hospital, 1250 Moursund Street, Suite 1325, Houston, Texas 77030, USA

Corresponding author:

Detlef Heck, Ph.D.

University of Tennessee Health Science Center

Dept. Anatomy & Neurobiology

855 Monroe Ave.

Memphis, TN 38163

Phone: +1 901 448 1678

E-mail: dheck@uthsc.edu

ABSTRACT

The medial prefrontal cortex (mPFC) and dorsal hippocampal CA1 region (dCA1) in rodents show increased coherence of neuronal oscillations during decisions in learned spatial working memory (SWM) tasks and the coherence changes reflect decision outcome. However, how coherence is controlled is unknown. We found in mice that decision related gamma coherence modulation between the mPFC and dCA1 and normal SWM performance required an intact cerebellum. Optogenetic activation of the cerebellar lobulus simplex impaired decision-related mPFC-dCA1 coherence modulation and SWM performance. Our findings reveal a role for the cerebellum in the task-specific modulation of coherence between cerebral cortical areas as possible mechanism of cerebellar cognitive function.

INTRODUCTION

Spatial navigation involves the integration of environmental and autogenous sensory cues to create internal representations of space. The maintenance of this mental representation to recall previously visited areas and to plan new paths accordingly is an essential form of spatial working memory (SWM). Place cells within the hippocampus encode position within a subject's perceived space, and thus are thought to provide a neuronal map that executive areas may reference for navigational decision-making. It has recently been shown that the cerebellum provides input to the hippocampus [1], and that this input is necessary for the stability of place cell mapping to be consistent environmental cues [2]. These findings suggest an essential role for the cerebellum in spatial working memory via the integration of external and internal sensory cues that help shape the neuronal representation of space in the hippocampus.

Integration of cues, as well as reference to the resulting neuronal map by executive areas, requires precise spatiotemporal coordination of neuronal activity between the medial prefrontal cortex (mPFC) and the dorsal hippocampus [3]. While the necessity of these areas for successful SWM has been known, the

neuronal mechanisms that support the task dependent coordination of neuronal communication between them remain unclear. The decision-making process during SWM tasks is associated with a brief increase in the coherence of neuronal oscillations in the mPFC and dorsal hippocampal CA1 region (dCA1), and this coherence increase is believed to be essential for normal SWM decision-making [3-6]. We recently reported that Purkinje cells in the cerebellar lobulus simplex (LS) and Crus I represent the phase and phase differences of neuronal oscillations in the mPFC and dCA1 [7]. We hypothesize that cerebellar output from the LS is essential for the normal modulation of decision-related mPFC-CA1 coherence and for normal SWM decision-making. We focus on the cerebellar LS because mPFC-dCA1 decision related coherence modulation occurred in the gamma band (80-90 Hz) and Purkinje cells in LS represented the phase of gamma oscillations in the mPFC and dCA1, while Purkinje cells in Crus I did not [7].

We performed electrophysiological recordings in the mPFC and dCA1(Fig. 1) in freely moving mice to evaluate SWM performance and decision-related mPFC-dCA1 coherence modulation during spontaneous exploration of a plus-maze. SWM performance was quantified by counting spontaneous alternations, i.e. sequences of arm entries without repeating entry into a recently visited arm [8, 9]. We then compared SWM performance and decision-related mPFC-dCA1 coherence modulation in control and mutant mice that have a selective loss of Purkinje cell neurotransmission to determine whether the cerebellum is required for SWM decision-making and decision-related mPFC-dCA1 coherence modulation. Optogenetic manipulation of LS Purkinje cell activity was used to determine whether Purkinje cell firing in the cerebellar LS is specifically and causally involved in SWM decision-making and decision-related mPFC-dCA1 coherence modulation. Our findings demonstrate a causal involvement of the LS in SWM decision making and, in the task-specific modulation of gamma coherence between the mPFC and dCA1.

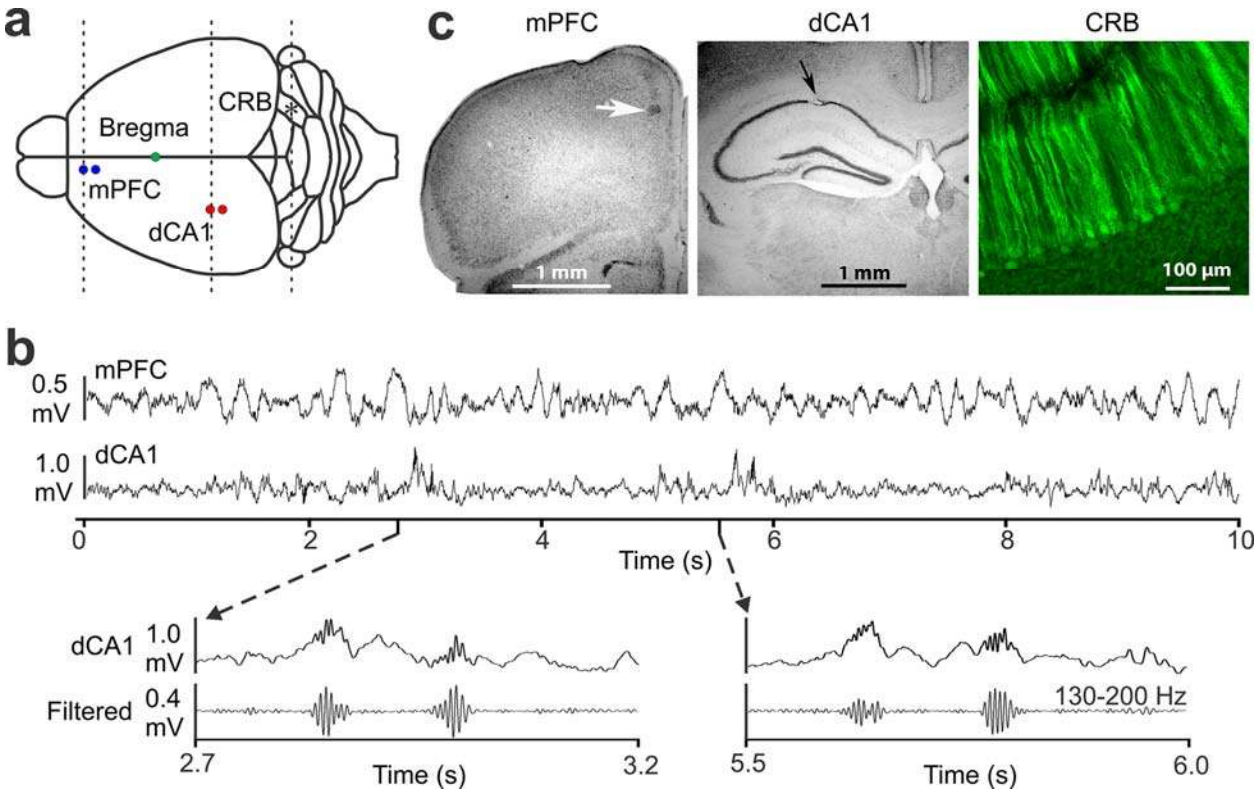

Figure 1. Illustration of recording locations in the mPFC and dCA1, example data and lesion sites. (**a**) Schematic drawing of the top view of a mouse brain. Local LFPs were recorded from the left mPFC and left CA1 region of the hippocampus (dCA1). The asterisk marks the site of optogenetic stimulation applied to the cortical surface of cerebellum (CRB). Dashed lines represent the approximate coronal sections for verifying the recording locations in mPFC and dCA1 as well as the ChR2 expression in Purkinje cells. (**b**) Examples of raw LFP signals recorded in mPFC and dCA1. Panels at the bottom show enlarged views of raw LFPs around ripple events in dCA1 (top traces) and band-pass filtered versions of the same LFP (130-200Hz) emphasizing the high-frequency component of sharp-wave ripple activity. (**c**) Examples of electrolytic lesions (arrows) at recording sites in the mPFC and dCA1 region and L7-Chr2-GFP expression in Purkinje cells of the LS.

RESULTS

Reduced plus-maze task performance in mice with functional cerebellar deficits

We measured SWM performance in $L7^{Cre};Vgat^{flox/flox}$ mice suffering from cerebellar ataxia induced by genetically-induced loss of Purkinje cell synaptic transmission [10] and compared their performance to unaffected $Vgat^{flox/flox}$ litter mates. A plus-maze behavioral test for SWM measuring spontaneous alternations [8] revealed a SWM deficit in $L7^{Cre};Vgat^{flox/flox}$ mice compared to their $Vgat^{flox/flox}$ control littermates and C57BL/6J mice (Fig. 2b). The C57BL/6J group consisted of non-transgenic C57BL/6J control mice (n = 5), and transgenic C57BL/6J mutant mice expressing channelrhodpsin-2 in cerebellar Purkinje cells (L7-ChR2$_{Chip,}$ n = 8; L7-ChR2$_{Fiber,}$ n = 9). SWM performance did not differ between the three ChR2 test groups and their behavioral results were pooled (C57BL/6J$_{Chip}$: 36.9% ± 2.2%; L7-ChR2$_{Chip}$: 34.6% ± 2.2%; L7-ChR2$_{Fiber}$: 38.3% ± 3.5%; Two-sample t-tests between groups: $p > 0.05$). SWM performance as expressed by the percentage of spontaneous alternations was comparable in C57BL/6J and $Vgat^{flox/flox}$ mice (36.7% ± 1.7% vs. 42.6%± 1.6%; p=0.112; two-sample t-test). By contrast $L7^{Cre};Vgat^{flox/flox}$ mice showed significantly reduced percentages of spontaneous alternations compared to their control littermates (21.2% ± 1.4% vs. 42.6% ± 1.6%, p=0.0001, two-sample t-test) and compared to C57BL/6J mice (21.2% ± 1.4% vs. 36.7% ± 1.7%, p=0.0002, two-sample t-test).

Abnormal coherence between mPFC and dCA1 during decision-making in cerebellar deficit mice

Decision-related changes in coherence between the mPFC and dCA1 have been implicated in the process of SWM decision-making [3, 14]. We analyzed time-resolved LFP coherence during the period of decision-making, i.e. from the time the mouse entered the center area of plus-maze until the time the mouse left the center and entered the chosen arm. We focused our analysis on data recorded during the two-second period before the mice exited the center area and entered the next arm. The time of exit from the center was defined as the time all four paws were inside the newly entered maze arm. A comparison of decision-related changes in mPFC-dCA1 coherence between $Vgat^{flox/flox}$ control mice and

L7^{Cre};*Vgat*$^{flox/flox}$ mutants revealed a correlation between SWM decision outcome and coherence modulation in *Vgat*$^{flox/flox}$ mice (Fig. 2c-e) but not in *L7*^{Cre};*Vgat*$^{flox/flox}$ mice (Fig. 2f-h). Decision-related coherence modulation in *Vgat*$^{flox/flox}$ control mice differed between correct and incorrect decisions at around 0.8 sec prior to the time of entering the next maze arm (Fig. 2e). By contrast, in *L7*^{Cre};*Vgat*$^{flox/flox}$ mutant mice the time courses of coherence during the decision process were similar for correct and incorrect decisions (Fig. 2h).

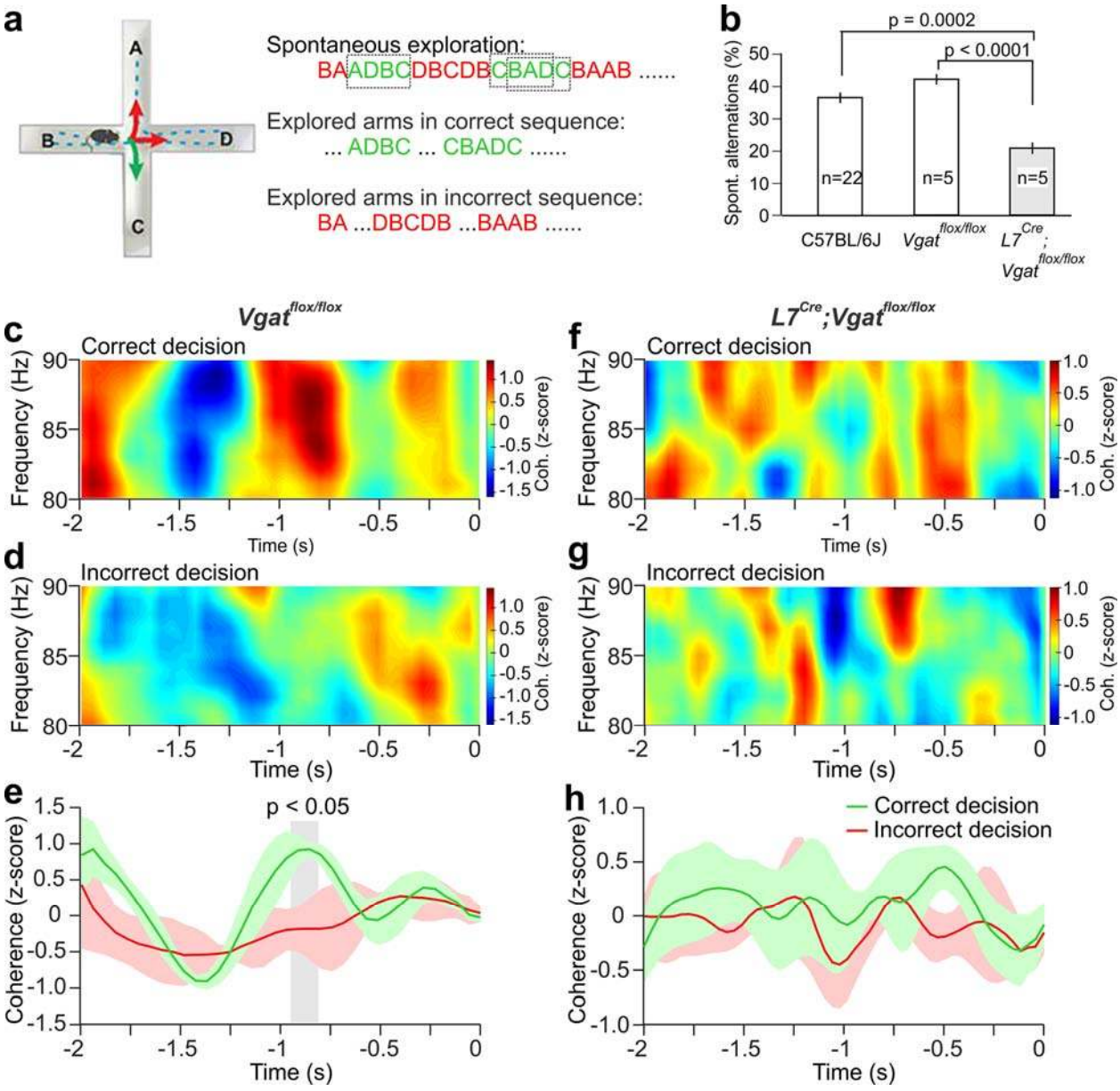

Figure 2. Spatial working memory performance and decision-related gamma coherence between the mPFC and dCA1 are impaired in mice with genetically-induced loss of Purkinje cell synaptic transmission. (**a**) Schematic drawing of a plus-maze with arms labeled by letters and example arm-entry sequences shown on the right. Four consecutive arm-entries without repeats are considered a spontaneous alternation and are shown as green letter sequences framed by dashed rectangles in the examples. Blue dashed line describes an example path with arm-entry sequence A-D-B with the mouse approaching the center area. Arrows illustrate the current choice situation, where the mouse is leaving arm B, entering A or D would be incorrect choices (red arrows) and entering arm C (green arrow) would be the correct choice and complete a spontaneous alternation. All arm-entries that are part of a spontaneous alternation are considered correct choices. Note that spontaneous alternation sequences can be overlapping. All other entries (red letters in the example sequences) are classified as incorrect choices. (**b**) Plus-maze SWM task performance comparison between healthy C57BL/6J mice, $Vgat^{flox/flox}$ control mice and mutant $L7^{Cre};Vgat^{flox/flox}$ mice. Bars represent mean percentage of spontaneous alternations in the sequence of arm entries. Error bars show ± standard error. P-values result from two-sample t-tests. (**c**) Pseudo-color plot showing decision-related changes in mPFC-dCA1 gamma (80-90 Hz) coherence in unaffected $Vgat^{flox/flox}$ control mice, averaged over 89 decisions. Time zero on the x-axis corresponds to the moment the mouse is leaving the center, defined as all four paws being inside the next chosen maze arm. (**d**) As in **c** but for incorrect decisions made by unaffected $Vgat^{flox/flox}$ control mice, averaged over 121 decisions. (**e**) Time courses of coherence for correct (green) and incorrect (red) decisions obtained by averaging results in **c** and **d** across the frequency range (80-90Hz). Shaded areas represent ± standard error. (**f - h**) As for **c - d** but for $L7^{Cre};Vgat^{flox/flox}$ mutant mice (including 31 correct and 115 incorrect decisions). Vertical gray bar in **e** indicates a time period where average coherence values differed between correct and incorrect decision ($p < 0.05$, paired t-tests).

Optogenetic activation of Purkinje cells in the LS during decision-making impairs SWM performance

We have previously shown that Purkinje cells in LS represent phase information of gamma oscillations in the mPFC and dCA1 [7]. After we identified changes in gamma coherence to be linked to SWM decision outcome, we asked whether a modulation of Purkinje cell activity specifically in the LS would alter SWM performance. As described in the method section, we used two types of LED light sources, a Chip-LED placed directly on the thinned bone overlying LS and a fiber-coupled LED with the tip of the fiber touching the dura overlying the LS. Photoactivation of LS Purkinje cells with either type of LED was controlled manually by the experimenter and occurred at the moment the mouse's nose entered the center of the plus maze and lasted for one second (see methods). Stimulation of LS Purkinje cells with either LED type caused a decrease in SWM performance to around chance levels (Fig. 3a,b). The percentage of spontaneous alternations dropped from 34.6% to 20.6% for mice stimulated with the Chip-LED (L7-ChR2$_{Chip}$, Fig. 3a) and from 38.3% to 24.3% for mice stimulated with the fiber-coupled LED (L7-ChR2$_{Fiber}$, Fig. 3b). When optical stimulation with a Chip-LED was applied to C57BL/6J mice that did not express channelrhodopsin-2 (C57BL/6J$_{Chip}$), we found no difference in SWM performance between stimulated and non-stimulated trials (36.9% vs. 39.0%; Fig. 3c).

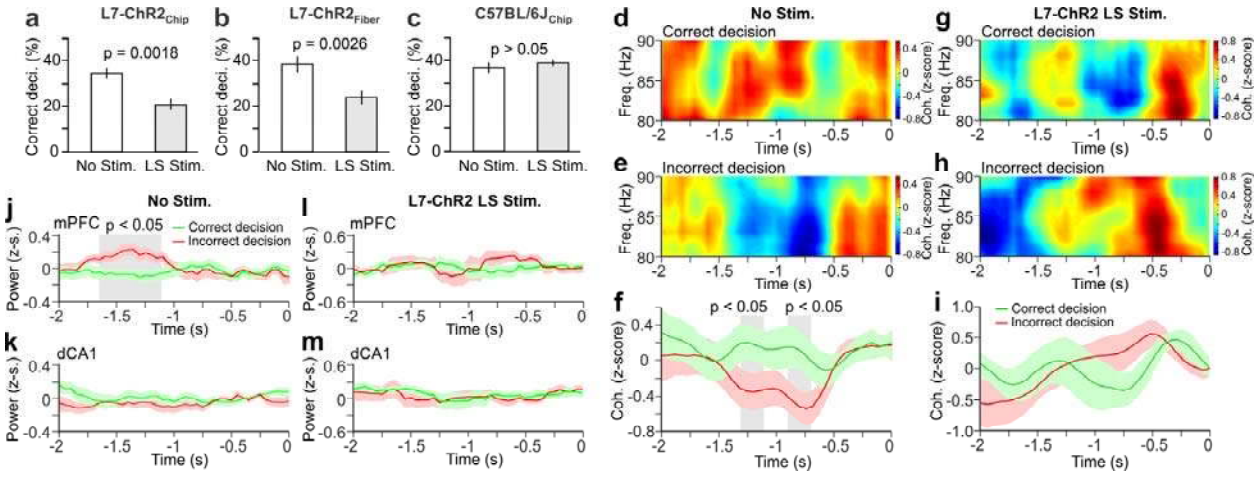

Figure 3. Optogenetic activation of Purkinje cells in the LS at the time of decision-making impairs plus-maze SWM performance, decision-related mPFC-dCA1 gamma coherence and gamma power in the mPFC. (**a**) Comparison of plus-maze trials without (No Stim) and with (LS Stim) optical stimulation with Chip-LED (L7-ChR2$_{Chip}$; n = 8). (**b**) Comparison of plus-maze trials without (No Stim) and with (LS Stim) optical stimulation with fiber-coupled LED (L7-ChR2$_{Fiber}$; n = 9). (**c**) Comparison of plus-maze trials without (No Stim) and with (LS Stim) illumination of the LS in C57BL/6J control mice that did not express ChR2 in Purkinje cells (C57BL/6J$_{Chip}$; n = 5). Data are expressed as mean ± standard error. P-values in **a** - **c** result from paired t-tests. (**d - i**) Time-resolved analysis of decision-related changes in mPFC-dCA1 gamma coherence during performance of the plus-maze SWM task with and without optical stimulation of Purkinje cells in the LS. Mice expressing channelrhodopsin-2 in Purkinje cells were implanted with a fiber-coupled LED (L7-ChR2$_{Fiber}$) overlying the LS for optical stimulation. (**d**) Pseudo-color plots of decision-related changes of mPFC-dCA1 gamma coherence during correct decisions. Time zero corresponds to the time the mouse is leaving the center area, i.e. all four paws have left the center and entered the next arm. (**e**) As in **d** but for incorrect decisions. (**f**) Average time course of gamma coherence modulation during correct (green) and incorrect (red) decisions obtained by averaging the coherence values in **d** and **e** across frequencies. Green and red shaded areas correspond to ± standard error (n = 20 consisting of: L7-ChR2$_{Chip}$ n = 7; L7-ChR2$_{Fiber}$ n = 9; C57BL/6J$_{Chip}$ n = 4). Gray shaded areas mark epochs of significant differences between the two coherence functions. (**g - i**) Decision-related coherence of mPFC-dCA1 gamma oscillations as in **d, e** and **f,** but for trials where LS Purkinje cells were optically activated during the decision-making process (n = 9). Data in **f** and **i** are expressed as mean ± standard error and P-values represent paired t-tests. (**j - m**) Time-frequency analysis of decision-related changes in gamma oscillation power in mPFC and dCA1 during decision-making in the plus-maze task, comparing power changes in trials with and without optical stimulation of Purkinje cells in the LS. (**j**) Time course of gamma power in the mPFC during plus-maze trials without optical stimulation (n=20). (**k**) As in **j** but for the dCA1. (**l**) Time course of gamma power in the mPFC during plus-maze trials where LS Purkinje cells

were optically activated during the SWM decision-making process (n=9). (**m**) As in **l** but for the dCA1. Gray shaded area in **j** marks epoch of significant differences between the two functions. Data in **j – m** are expressed as mean ± standard error and P-values represent paired t-tests.

Optogenetic activation of Purkinje cells in the LS impairs mPFC-dCA1 decision-related coherence modulation

We next evaluated how optical stimulation of Purkinje cells in the LS of L7-ChR2$_{Fiber}$ mice at the time of decision-making would affect SWM performance, decision-related mPFC-dCA1 coherence and the power of gamma oscillations in the mPFC and dCA1. Coherence analysis of plus-maze trials without optical stimulation again revealed coherence modulation patterns that differed between correct and incorrect decisions (Fig. 3d-f). Similar to *Vgat*$^{flox/flox}$ control mice, coherence increased to higher values for correct vs. incorrect decisions at 1.1-1.3 sec prior to the mouse leaving the center of the maze (Fig. 3f). In L7-ChR2 mice we found a second time period of significantly elevated coherence during correct decisions at 0.7-0.9 sec prior to leaving the center (Fig. 3f). Optical stimulation of LS Purkinje cells during decision-making eliminated all decision-related differences in mPFC-dCA1 coherence modulation (Fig. 3g-i).

Time-frequency analysis of mPFC and dCA1 gamma oscillations during control trials without optical stimulation revealed an increase in mPFC gamma power during incorrect but not during correct decisions (Fig. 3j). We did not observe any decision-related modulation of gamma power in the dCA1 (Fig. 3k). Optical stimulation of LS Purkinje cells during the decision-making process eliminated the increase in mPFC gamma power during incorrect decisions but did not cause any change in gamma power during correct decisions (Fig. 3l). Optical stimulation of LS Purkinje cells during decision-making had no effect on gamma power in dCA1 (Fig. 3m).

DISCUSSION

The cerebellum has been implicated in a broad spectrum of cognitive functions, and extensive connections between the cerebellum and association cerebral cortical areas likely provide the anatomical basis for cerebrocerebellar interactions [15, 16]. However, the neuronal mechanism of cerebrocerebellar communication remain unknown. Cerebellar connections with the prefrontal cortex have long been implicated in cerebellar cognitive function [17] and the more recently discovered connections between the cerebellum and hippocampus [1] are likely a key anatomical substrate for cerebellar involvement in spatial functions [2, 18]. The prefrontal cortex and hippocampus, specifically the medial prefrontal cortex (mPFC) and dorsal hippocampus region (dCA1) in rodents are jointly required for spatial working memory (SWM) [14, 19-21]. Here we present causal evidence for an involvement of the cerebellar lobulus simplex (LS) in the decision-making process in a SWM task and in the modulation of decision-related gamma coherence modulation in the mPFC and dCA1.

A first behavioral comparison of SWM performance between $L7^{Cre};Vgat^{flox/flox}$ mice with genetically induced, cerebellum-wide loss of Purkinje cell GABAergic neurotransmission with their unaffected $Vgat^{flox/flox}$ control littermates and healthy C67BL/6J mice revealed a significant SWM performance deficit in $L7^{Cre};Vgat^{flox/flox}$ mice (Fig. 2b), suggesting that an intact cerebellum is required for normal SWM. A comparison of coherence modulation for correct and incorrect SWM decisions showed higher magnitude mPFC-dCA1 gamma coherence increase for correct decisions in $Vgat^{flox/flox}$ control mice but not in $L7^{Cre};Vgat^{flox/flox}$ mutants (Fig. 2e,h), suggesting that decision-related mPFC-dCA1 coherence modulation requires an intact and fully functional cerebellum.

Purkinje cells in the cerebellar lobulus simplex (LS) have been shown to represent gamma oscillation phase in both the mPFC and dCA1 [7], suggesting a potential involvement of LS Purkinje cell

activity in mPFC-dCA1 gamma coherence. Optogenetic stimulation of LS Purkinje cells during the time of decision-making significantly impaired SWM performance compared to trials without stimulation (Fig. 3a-c). Similarly, decision-outcome related differences in mPFC-dCA1 gamma coherence observed in trials without stimulation (Fig. 3d-f), were eliminated when LS Purkinje cells were activated during decision-making (Fig. 3g-i). These findings reveal a causal involvement of the cerebellar LS in SWM decision making and in the modulation of decision-related mPFC-dCA1 gamma coherence.

In addition, analysis of gamma oscillation power during SWM decision-making revealed an increase in gamma power in the mPFC during incorrect but not during correct decisions, with no decision-related changes in gamma power in the dCA1 (Fig. 3j,k). Optical stimulation of LS Purkinje cells showed that LS stimulation eliminated the increase in mPFC gamma power during incorrect decisions while having no effect on gamma power during correct decisions or on gamma power in the dCA1 (Fig. 3l,m). These findings suggest that LS Purkinje cell activity selectively influences gamma power in the mPFC and not dCA1. LS stimulation did not alter mPFC gamma power during correct decisions, suggesting that the influence of LS on mPFC gamma power is strictly context dependent. In this case, the role of the cerebellum could be interpreted as focusing mPFC neuronal processing on SWM decision-making by suppressing disruptive mPFC gamma activity possibly driven by decision-unrelated inputs.

We observed no decision-related modulation of mPFC gamma power in $L7^{Cre};Vgat^{flox/flox}$ and $Vgat^{flox/flox}$ mice (Supplementary Fig. 1). Lack of decision-related gamma power modulation in these mice may be due to the smaller number of animals we tested in that group, but it is also possible that strain differences play a role. However, decision-related mPFC-dCA1 coherence modulation was observed in $Vgat^{flox/flox}$, C57BL/6J and L7-Chr2 mice alike, indicating that a cerebellar involvement in the modulation of cerebral cortical oscillation power and coherence is likely realized via independent mechanisms.

The modulation of coherence has been proposed as a mechanism for the precise spatial and temporal coordinating neuronal communication between cerebral cortical areas during cognitive

processes [22, 23]. This proposed principle has since been extended to include sensory motor processing and corticospinal communication and it has received substantial support from experimental findings [24-27]. However, what mechanisms control the timing and magnitude of coherence changes between crucial brain areas during specific tasks remains unknown. Here we propose that that the cerebellum plays a key role in the task dependent modulation of coherence of oscillations between specific cerebral cortical areas, thus contributing to a task dependent coordination of neuronal communication between cerebral cortical structures. The findings presented here relate to a cognitive task. However, Popa et al. have shown that the cerebellum is also required for normal gamma coherence between sensory and motor cortical areas in the mouse [28], and Lindeman et al. recently reported evidence of cerebellar modulation of coherence between the sensory and motor cortical areas in the mouse linked to whisking behavior [29]. Cerebellar coordination of cerebral-cortical coherence could thus represent a universal principle of cerebrocerebellar neuronal interaction, applicable to both cerebellar cognitive and sensorimotor functions. Although this proposed cerebellar function provides a novel view of cerebrocerebellar interaction, the coordination of phase-relationships between two oscillations is a temporal coordination problem and thus very much in line with traditional views of the cerebellum as a structure specializing in the analysis and coordination of precisely timed events [30-33].

METHODS

Animals

Thirty-two adult mice (18 males; 14 females) from 3 different strains were used in this study. One strain consisted of ataxic mice with genetically induced loss of Purkinje cell GABAergic neurotransmission ($L7^{Cre};Vgat^{flox/flox}$, n = 5) and their unaffected littermate controls ($Vgat^{flox/flox}$, n = 5) [10]. A second strain selectively expressed channelrhodopsin-2 (ChR2) in cerebellar Purkinje cells (Tg(Pcp2-

COP4*H134R/EYFP)U126Isop/J) and was used for optophysiological activation of Purkinje cells in the LS. C57BL/6J mice served as an additional control. Table 1 summarizes the experimental groups, manipulations and analyses that were carried out. Mice used of optogenetic stimulation were divided into two groups as we used two different light sources, a Chip-LED (L7-ChR2$_{Chip}$, n = 8) and an optical fiber-coupled LED (L7-ChR2$_{Fiber}$, n = 9). C57BL/6J mice served as controls for optical stimulation with the LED Chip in the absence of ChR2 expression (C57BL/6J$_{Chip}$, n = 5).

Electrophysiological recordings of local field potentials in the mPFC and dCA1 were performed in all mice and time resolved coherence analysis was used to evaluate decision-related changes in coherence of neuronal oscillations (see below). One mouse in the L7-ChR2$_{Chip}$ group and one in the C57BL/6J$_{Chip}$ control group did not provide usable electrophysiological data. Electrophysiological data from these two mice and were excluded from coherence analysis but their behavioral data were included in the analysis of SWM performance (asterisks in Table 1).

Table 1. Experimental groups and treatments. *L7^{Cre};Vgat$^{flox/flox}$*: ataxic mutants, *Vgat$^{flox/flox}$*: non-ataxic control littermates; L7-ChR2$_{Chip/Fiber}$: mice expressing channelrhodopsin-2 in cerebellar Purkinje cells.

Group	n (M/F)	SWM test	Coherence analysis (no stimulation)	Coherence analysis w/opt. stim.	Light source	Opt. Stimulation frequency
L7^{Cre};Vgat$^{flox/flox}$	5 (5/0)	+	+			
Vgat$^{flox/flox}$	5 (1/4)	+	+			
L7-ChR2$_{Chip}$	8* (5/3)	+	+		Chip-LED	100 Hz
L7-ChR2$_{Fiber}$	9 (4/5)	+	+	+	Fiber-LED	120 Hz
C57BL/6J$_{Chip}$	5* (3/2)	+	+		Chip-LED	120 Hz

* One mouse each from the L7-ChR2$_{Chip}$ and C57BL/6J$_{Chip}$ groups were included in the analysis of behavior but excluded for coherence analysis due to unsuccessful electrophysiological recordings.

Mice were housed in a breeding colony at the University of Tennessee Health Science Center animal facilities with 12-hour light/dark cycles in standard cages with free access to food and water. All animal procedures were performed in accordance with the NIH Guide for the Care and Use of Laboratory Animals (2011). Experimental protocols were approved by the Institutional Animal Care and Use Committee at the University of Tennessee Health Science Center.

Surgery

Mice were surgically prepared for freely moving electrophysiological recordings in the mPFC and dCA1 (Fig. 1). Surgical anesthesia was initiated by exposing mice to 3% isoflurane in oxygen in an induction chamber. Anesthesia was maintained with 1-2% isoflurane in oxygen during surgery using an Ohio isoflurane vaporizer (Highland Medical Equipment, Deerfield, IL, USA). Body temperature was maintained at 37-38˚C with a servo-controlled heat blanket (FHC, Bowdoinham, ME, USA) monitored by rectal thermometer. At the beginning of each surgery, after mice were anesthetized but before the first incision, mice received a single subcutaneous injection of the analgesic Meloxicam SR (4 mg/kg, 0.06 ml) to alleviate pain. Two round openings (1.0 mm diameter) were prepared in the skull bone overlying the left mPFC (AP 2.46 mm; ML 0.5 mm) and the left hippocampus (AP -2.3 mm; ML 2.0 mm) (Fig. 1a) using a dental drill (Microtorque II, RAM Products, Inc., USA), leaving the underlying dura intact. For mice receiving optical stimulation with a Chip-LED (L7-ChR2$_{Chip}$ and C57BL/6J$_{Chip}$) the bone overlying the right cerebellar LS (AP -6.0 mm; ML 2.0 mm) was thinned and the Chip-LED placed directly on the thinned bone. For receiving optical stimulation via an optical fiber-coupled LED (L7-ChR2$_{Fiber}$) a small opening was prepared overlying the LS and the fiber was fixed in place to touch but not penetrate the dura. Two extracellular recording electrodes (glass insulated tungsten/platinum; 80 μm diameter; impedance:

3.5-5.0 MΩ) attached to a custom-made micro-drive were centered over the mPFC and dCA1 skull openings and the micro-drives were fixed to the skull using dental cement. The four electrodes, a reference wire and a ground wire were then connected to a 20-pin micro-connector (Omnetics Connector Corp.). Mice in the L7-ChR2$_{Chip}$, L7-ChR2$_{Fiber}$ and C57BL/6J$_{Chip}$ groups received additional implants of a chip-LED or an LED-coupled optical fiber (see below for technical details on LEDs) over the cerebellar LS. Two miniature female gold plugs were used to deliver power to the LEDs via a thin wire (2 m, 40 AWG solid nickel). Finally, an acrylic head-post was mounted on the skull to provide a handle to manually stabilize the head while connecting and disconnecting the wireless headstage. The micro-drives, head-post and wire connectors were embedded in dental cement and anchored to the skull bone using three small skull screws. Of those, one on the right side (AP -1 mm; ML 3 mm) was connected with the reference wire and one on the left side (AP -4 mm; ML 4 mm) was used as a ground. A postsurgical recovery period of 3-4 days was allowed before electrophysiological experiments began.

Electrophysiology

Electrophysiological recordings were conducted with extracellular recording electrodes (glass insulated tungsten/platinum; 80 µm diameter; impedance: 3.5-5.0 MΩ) attached to a custom-made micro-drive. Two electrodes each, separated by 0.25 mm, were placed in the mPFC and dCA1. All four electrodes were connected to a 20-pin micro-connector (Omnetics Connector Corporation). During recording sessions, a wireless headstage (W2100-HS16, Multichannel Systems, Germany) was plugged into the miroconnector. To reduce weight the battery was kept off the head stage and power was supplied by connecting the battery and head stage with two highly flexible thin wires (2 m, 40 AWG solid nickel). Recordings were performed on five consecutive days. On the first day, electrodes were manually advanced into the left mPFC and dCA1 while the animals were in their home-cage. The occurrence of sharp wave ripples (SWR) were used to determine electrode tip placement in dCA1 [11] (Fig. 1b). On subsequent days, recordings were performed during plus maze testing and electrode positions were only

altered in the dCA1 if SWR signals were lost. Broad band voltage signals (0.1 – 8 kHz) were digitized at 20 kHz and saved to a hard-disk (W2100-HS16, Multichannel Systems, Germany). LFPs were band-pass filtered off-line at 0.1 – 200 Hz using Spike2 software (Cambridge Electronic Design Limited, UK). After completion of the final experiment, recording sites were marked by small electrolytic lesions (10 µA DC; 12 s) and verified anatomically (Fig. 1c).

Behavioral task

The plus-maze task was used to quantify SWM using counts of spontaneous alternations [8]. During spontaneous maze exploration, healthy mice tend to avoid entering recently visited arms and generate arm-entry sequences without repetition at above-chance level. Such repeat-free sequences called spontaneous alternations (Fig. 2a). In a four-arm maze, like the plus-maze used here, random arm visits would result in 22.5% spontaneous alternations. Healthy mice or rats generate significantly higher numbers of spontaneous alternations and a decrease in spontaneous alternations is interpreted as a deficit in SWM [8, 9]. Mice explored the plus-maze for 12 min while their arm entry sequence was automatically tracked with a video system (30 frames/s; Viewer, Biobserve GmbH). Arm entry sequences and resulting spontaneous alternations were analyzed off-line.

Each mouse performed the plus-maze test 5 times, once per day, on five successive days. The first session was to allow mice to become familiar with the maze and was not analyzed further. On the four subsequent days, electrophysiological recordings were performed during each session and mouse movements were tracked by video. Mice in three groups were prepared to also receive optical stimuli to the cerebellar LS at the time of decision-making (L7-ChR2$_{Chip}$, L7-ChR2$_{Fiber,}$ C57BL/6J$_{Chip}$). We alternated between days with and without optical stimulation. Whether optical stimulation was applied on days 1 and 3 or days 2 and 4 was pseudo-randomized. Each arm entry was classified as 'correct' or 'incorrect' based on whether it was part of a spontaneous alternation sequence or a repeat entry (Fig. 2a).

Optogenetic stimulation

During the decision phases of plus-maze trials with cerebellar optical stimulation, Purkinje cells in the LS of L7-ChR2 expressing mice and a control group of C57BL/6J mice were exposed to a 1 sec light stimulus (sinusoidally modulated illumination, 100 Hz or 120 Hz). Sinusoidal modulation of light stimuli was chosen to avoid the possibility of a depolarization block to occur with sustained DC illumination. The light modulation frequency was chosen to fall outside the frequency range of interest for coherence analysis and elevated from 100 Hz to 120 Hz when high gamma oscillations between 80 and 90 Hz were identified as the frequency band of interest. The sinewave voltage used to control LED illumination was digitized (2 kHz) and recorded simultaneously with the electrophysiological data. Onset of the light stimulus was timed manually to occur at the moment the mouse's nose entering the center area of the plus maze. Two different LED devices, both emitting 465 nm light, were used for optical stimulation. A chip/micro SMD LED (1.25 x 2 mm, Lighthouse LEDs, LLC, WA, part # 10X12V0805PREWIREDBLUE) was used for optical stimulation in 8 L7-ChR2$_{Chip}$ mice and 5 C57BL/6J$_{Chip}$ mice. The Chip-LED was placed directly on the thinned bone overlying the LS and held in place with acrylic cement. Stimulation with the Chip-LED turned out to generate large artifacts in the electrophysiological signals. Electrophysiological data from the L7-ChR2$_{Chip}$ group were therefore excluded from further analysis of coherence modulation. We switched to using LEDs mounted on a 5 mm long optical fiber (200 micrometers diameter, Doric Lenses Inc., Quebec, Canada) for optical stimulation in 9 ChR2 expressing mice, with the optical fiber placed directly on the cortical surface of the LS without penetrating the dura. This method generated no significant electrical artifacts in LFP recordings and

allowed the analysis of mPFC-dCA1 coherence during trials with optical stimulation. Optical stimulation with the two different light sources generated the same effects on behavior.

Data analysis

Raw data processing: Raw electrophysiological data were first processed to remove power-line interference (60 Hz and harmonics) using a spectrum interpolation method [12, 13]. Data were then low pass filtered to create LFPs for further analysis (cutoff frequency: 200 Hz). All LFP signals were aligned at the time point that marked the moment the mice left the center area (time 0 in all time-resolved plots), defined by all four paws being outside the center square and inside the newly chosen arm. For each task trial, ten seconds of LFP data centered on time 0 were selected and stored to a hard disk (at 2 kHz). The LFP data of L7-ChR2$_{Chip}$ group which received optical cerebellar stimulation with light modulated at 100 Hz were excluded from analyzing the stimulation effect on LFP coherence because the frequency of the stimulation was too close to the high gamma frequency band (80-90 Hz). The light modulation frequency was increased to 120 Hz in subsequent experiments to avoid this problem.

Time-resolved coherence analysis of LFP: Of the two LFP signals available from two recording sites in each the mPFC and in the dCA1, one signal was chosen for further analysis. In the dCA1 we chose the LFP with the highest amplitude SWRs for further analysis, unless there was no difference, in which case one signal was chosen at random. In the mPFC, if LFP signals were equal in quality and one was chosen at random. In both the dCA1 and the mPFC recordings, if one signal showing increased line noise or artifacts, the other was used. All LFP data were first z-scored (Matlab function code: zscore).

Time-resolved coherence was calculated in Matlab using custom scripts (Matlab R2019b; function code: *mscohere*; sliding window: 1 s; step size: 20 ms).

Time-frequency analysis of LFP: To examine time-frequency aspects of LFP activity in the mPFC and dCA1 region of the hippocampus, the same z-scored LFP data that were used for coherence analyses were used to conduct a time-frequency analysis, using custom scripts based on the Matlab function code: *pspectrum*. The temporal resolution of the time resolved analysis was 0.2 s.

Statistical analyses: All data collected for specific experimental paradigms were averaged for each mouse. Paired t-test, Two-Sample t-test and Wilcoxon rank sum test were used to analyze changes in behavioral results from the plus-maze task as well as for coherence and power spectrum of LFP activities in the mPFC and dCA1. Figures represent results as mean ± standard error.

Histological evaluation of recording location

At the end of the experiments, animals were deeply anesthetized with intraperitoneal injection of Avertin (Tribromoethanol, 500 mg/kg) and intracardially perfused with 0.9% NaCl and followed by 4% paraformaldehyde solution. Brains were removed from the skull and post-fixed in 4% paraformaldehyde solution for a minimum of 24 hours. Fixed brains were then sectioned at 60 μm, mounted onto glass slides and Nissl stained. Light microscopy was used to localize electrolytic lesions and verify the correct placement of the recording electrode tip in the mPFC and the dCA1 (Fig. 1c).

REFERENCES

1. Watson, T.C., *et al.* Anatomical and physiological foundations of cerebello-hippocampal interaction. *eLife* **8** (2019).
2. Lefort, J.M., *et al.* Impaired cerebellar Purkinje cell potentiation generates unstable spatial map orientation and inaccurate navigation. *Nat Commun* **10**, 2251 (2019).
3. Spellman, T., *et al.* Hippocampal-prefrontal input supports spatial encoding in working memory. *Nature* **522**, 309-314 (2015).
4. Gordon, J.A. Oscillations and hippocampal-prefrontal synchrony. *Curr Opin Neurobiol* **21**, 486-491 (2011).
5. Lee, I. & Kesner, R.P. Time-dependent relationship between the dorsal hippocampus and the prefrontal cortex in spatial memory. *J Neurosci* **23**, 1517-1523 (2003).
6. Churchwell, J.C. & Kesner, R.P. Hippocampal-prefrontal dynamics in spatial working memory: interactions and independent parallel processing. *Behav Brain Res* **225**, 389-395 (2011).
7. McAfee, S., Liu, Y., Sillitoe, R.V. & Heck, D.H. Cerebellar lobulus simplex and Crus I differentially represent phase and phase difference of prefrontal cortical and hippocampal oscillations. *Cell reports* **27**, 2328–2334 (2019).
8. Richman, C.L., Dember, W.N. & Kim, P. Spontaneous Alternation Behavior in Animals: A Review. *Current Psychological Research & Reviews* **5**, 358-391 (1987).
9. Lalonde, R. The neurobiological basis of spontaneous alternation. *Neurosci Biobehav Rev* **26**, 91-104 (2002).
10. White, J.J., *et al.* Cerebellar zonal patterning relies on purkinje cell neurotransmission. *J Neurosci* **34**, 8231-8245 (2014).
11. Buzsaki, G. Hippocampal sharp wave-ripple: A cognitive biomarker for episodic memory and planning. *Hippocampus* **25**, 1073-1188 (2015).
12. Mewett, D.T., Reynolds, K.J. & Nazeran, H. Reducing power line interference in digitised electromyogram recordings by spectrum interpolation. *Medical & biological engineering & computing* **42**, 524-531 (2004).
13. Leske, S. & Dalal, S.S. Reducing power line noise in EEG and MEG data via spectrum interpolation. *Neuroimage* **189**, 763-776 (2019).

14. Jones, M.W. & Wilson, M.A. Theta rhythms coordinate hippocampal-prefrontal interactions in a spatial memory task. *PLoS Biol* **3**, e402 (2005).

15. Schmahmann, J.D. The cerebellum and cognition. *Neurosci Lett* **688**, 62-75 (2019).

16. Buckner, R.L. The cerebellum and cognitive function: 25 years of insight from anatomy and neuroimaging. *Neuron* **80**, 807-815 (2013).

17. Middleton, F.A. & Strick, P.L. Cerebellar projections to the prefrontal cortex of the primate. *Journal of Neuroscience* **21**, 700-712 (2001).

18. Lefort, J.M., Rochefort, C., Rondi-Reig, L., Group of, L.R.R.i.m.o.B.-P.L. & Foundation, E.N.P. Cerebellar contribution to spatial navigation: new insights into potential mechanisms. *Cerebellum* **14**, 59-62 (2015).

19. Negron-Oyarzo, I.*, et al.* Coordinated prefrontal-hippocampal activity and navigation strategy-related prefrontal firing during spatial memory formation. *Proc Natl Acad Sci U S A* **115**, 7123-7128 (2018).

20. Wirt, R.A. & Hyman, J.M. Integrating Spatial Working Memory and Remote Memory: Interactions between the Medial Prefrontal Cortex and Hippocampus. *Brain Sci* **7** (2017).

21. Benchenane, K., Tiesinga, P.H. & Battaglia, F.P. Oscillations in the prefrontal cortex: a gateway to memory and attention. *Curr Opin Neurobiol* **21**, 475-485 (2011).

22. Womelsdorf, T.*, et al.* Modulation of neuronal interactions through neuronal synchronization. *Science* **316**, 1609-1612 (2007).

23. Fries, P. A mechanism for cognitive dynamics: neuronal communication through neuronal coherence. *Trends Cogn Sci.* **9**, 474-480 (2005).

24. Brunet, N.M.*, et al.* Stimulus repetition modulates gamma-band synchronization in primate visual cortex. *Proc Natl Acad Sci U S A* (2014).

25. McAfee, S.S., Liu, Y., Dhamala, M. & Heck, D.H. Thalamocortical transmission of visual information in mice involves synchronized spiking aligned with high gamma oscillations. *Front Neurosci* **12** (2018).

26. Bosman, C.A.*, et al.* Attentional stimulus selection through selective synchronization between monkey visual areas. *Neuron* **75**, 875-888 (2012).

27. Siegel, M., Donner, T.H., Oostenveld, R., Fries, P. & Engel, A.K. Neuronal synchronization along the dorsal visual pathway reflects the focus of spatial attention. *Neuron* **60**, 709-719 (2008).

28. Popa, D.*, et al.* Functional role of the cerebellum in gamma-band synchronization of the sensory and motor cortices. *J Neurosci* **33**, 6552-6556 (2013).

29. Lindeman, S.*, et al.* Cerebellar Purkinje cells can differentially modulate coherence between sensory and motor cortex depending on region and behavior. *bioRxiv*, 2020.2003.2011.986943 (2020).

30. Raghavan, R.T., Prevosto, V. & Sommer, M.A. Contribution of Cerebellar Loops to Action Timing. *Curr Opin Behav Sci* **8**, 28-34 (2016).

31. Ivry, R.B. & Spencer, R.M. The neural representation of time. *Current Opinion in Neurobiology* **14**, 225-232 (2004).

32. Braitenberg, V., Heck, D.H. & Sultan, F. The detection and generation of sequences as a key to cerebellar function. Experiments and theory. *Behav.Brain Sci.* **20**, 229-245 (1997).

33. Diener, H.C.*, et al.* The coordination of posture and voluntary movement in patients with cerebellar dysfunction. *Mov Disord.* **7**, 14-22 (1992).

ACKNOWLEDGEMENTS

D.H.H. and Y.L. are supported by R01MH112143, R01MH112143-02S1 and R37MH085726. R.V.S. is supported by R01NS089664, R01NS100874, R01MH112143 and U54HD083092. We would like to thank the Neuroscience Institute of the University of Tennessee Health Science Center (UTHSC) for financial support and Micheal Nguyen from the UTHSC Bio-Medical Services for technical support.

SUPPLEMANTARY MATERIAL

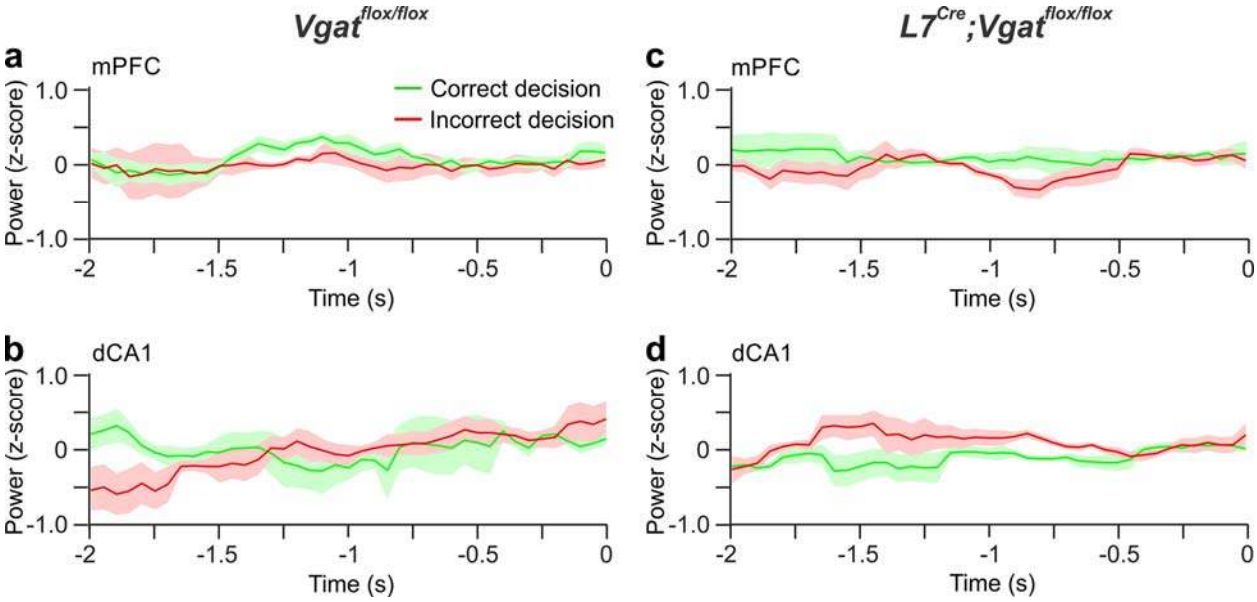

Supplementary Figure 1. Time-frequency analysis of decision-related changes in gamma oscillation power in the mPFC and dCA1 during performance of the plus-maze SWM task. Time axis is as in Figure 4 with time zero corresponding to the moment the mouse has left the center zone. (**a**) Time course of gamma power in the mPFC of $Vgat^{flox/flox}$ control mice. (**b**) As in **a**, but for the dCA1. (**c**) Time course of gamma power in the mPFC of ataxic $L7^{Cre};Vgat^{flox/flox}$ mutant mice. (**d**) As in **c** but for the dCA1. Data are expressed as mean ± standard error. In no case did gamma power differ between correct and incorrect decisions (paired t-test).